




## Self-damping of Optical Ground Wire Cables: A Bayesian Approach

Damián Federico Campos<sup>1</sup>, Enrique Eduardo Löser<sup>1</sup>, Marcelo Tullio Piovan<sup>2</sup>

<sup>1</sup> Conductor Testing Laboratory, Department of Applied Mechanics, Faculty of Engineering, Universidad Nacional del Comahue, Buenos Aires 1400, Neuquén, 8300, Argentina

<sup>2</sup> Center for Theoretical and Applied Research in Mechanics, Universidad Tecnológica Nacional FRBB, 11 de Abril 461, 8000, Bahía Blanca, Argentina

Received May 20 2022; Revised July 12 2022; Accepted for publication August 02 2022.

Corresponding author: D.F. Campos (damian.campos@fain.uncoma.edu.ar)

© 2022 Published by Shahid Chamran University of Ahvaz

**Abstract.** The empirical Power Law model has a long usage history in cable self-damping studies, and several types of research have been done to characterize its parameters for various types of cables. In this work, a novel Bayesian model calibration framework is proposed and applied to study self-damping Optical Ground Wire (OPGW) cables. This technique then combines experimental and statistical approaches to obtain the confidence intervals for each parameter and characterize the different regions where the model presents other behaviors. The results enable a better calibration of the model's parameters and agree with the trends already set in the literature. They also provide a new understanding of the model and estimate different uncertainties its application entices.

**Keywords:** Bayesian inference, self-damping, aeolian vibrations, uncertainty quantification, OPGW cables.

### 1. Introduction

Optical Ground Wire (OPGW) cables protect the power transmission line from atmospheric electrical discharges and data transmission [1]. Indeed, overhead transmission lines are mechanical structures with a large extent of slender and flexible elements, which lets them be highly exposed to wind [2]. Configuration details are shown in Fig. 1. Vibrations produced by the wind can be analyzed, in principle, according to the configuration of the line. If the line has only one conductor per phase or in the guard wire, the fundamental cause of vibration is the release of vortices, and the phenomenon is called aeolian vibration [3].

The phenomenon of aeolian vibrations in single cables produced by Von Karman vortex shedding is well known [4-6]. They generate small alternating forces on the cables in the normal wind direction. Aeolian vibrations are movements of small amplitude and high frequency (between 5 and 100 Hz) that constitute one of the main problems in transmission lines since they frequently lead to fatigue cracking in the wires of the cables or accessories for support and protection. The components that deserve special attention are the suspension and damping clamps [7].

Stockbridge and spiral-type dampers are employed to keep the vibration of the cables within safe levels. Therefore, studies that analyze the dynamic behavior of the OPGW cable with and without dampers become necessary [8].

The self-damping capacity of cables is a physical characteristic that defines their ability to dissipate energy internally while vibrating. For conventional stranded cables, energy dissipation is attributed mainly to friction due to small movements between overlapping strands when the cable is flexed, and this friction implies energy losses in the form of heat. Since larger cables have a greater contact surface between strands, they have better self-damping capacity [9-11].

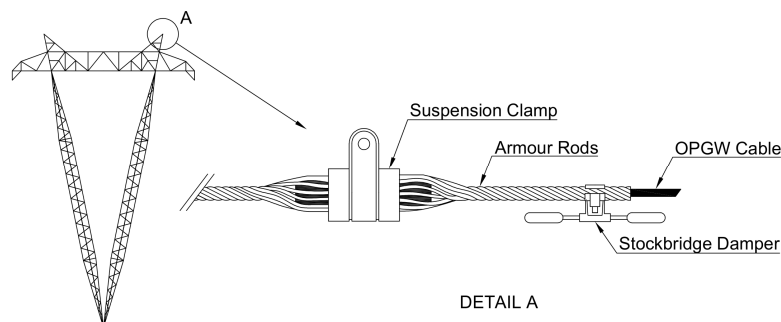


Fig. 1. Schematic representation of an Overhead Power Transmission Line (left) and OPGW cable installation scheme (right).

Experimental testing on laboratory spans is the target of international standards to get the identification of empirical equations in order to predict the self-damping capacity of cables and conductors of the same family (i.e., ACSR, OPGW) [12, 13]. According to these equations, the relationship between the cables' self-damping capacity, the amplitude and frequency of vibration, and the cable tension constitute a power law. The exponent coefficients are usually obtained from least-squares estimations of the experimental data collected in the tests. The standards fix the main features of the experimental setup, and it should be noted that the methodologies proposed there do not provide guidelines and requirements for the uncertainty and sensitivity of the transducers to be used. This has brought about a notable dispersion of the data collected by various research. Another drawback observed in these methods is that it is difficult to ensure the reproducibility between different studies. There is a quite substantial need for a technique that allows a more in-depth treatment of these results and to produce more informed decisions about the cable's self-damping and related phenomena. This technique is uncertainty quantification. One must first tackle the different types and sources of uncertainty to understand it. According to Oberkampf and Roy [14], sound taxonomies of uncertainties should try to classify them using their fundamental essence and then state how those categories of uncertainty are embodied in the studied model. Decades of research in this field have agreed upon the existence of two (sometimes overlapping) categories of uncertainty, and these are: aleatory and epistemic uncertainties.

Aleatory uncertainties are, as their name suggests, the outcome of a stochastic process. The most widely used model for this type of uncertainty is that of parametric uncertainty, i.e., Aleatory uncertainty in parameters can occur in the mathematical description of the system and its characteristics, initial conditions, boundary conditions, or excitation function. For this paper, aleatory uncertainty will play a part mainly in the recreation of boundary conditions for each measurement, and since measurement devices are a part of the system, they are also subject to aleatory uncertainty. This type of uncertainty may be controlled by identifying the potential sources of variability and actively trying to limit them. In this case, actions had to be taken to control the tension of the conductor as well as the frequency (and ramp-up to that frequency) that the conductor was shaken too.

The other type of uncertainty, Epistemic, is due to a lack of knowledge. This means that the observer has incomplete or incorrect information about the modeled system, affecting the observer's decisions and interpretations of the results. Epistemic uncertainty may influence every process step, from the experimental setup and data processing data to the specific algorithms and intermediate approximations used to get the desired system response. For this case, Epistemic uncertainty arises mainly because of the complex mechanism that the self-damping of a cable implies. Non-linear contact mechanics are in play, making using an empiric Power Law model a decision that should be tested. The purpose of the paper is to lay the basis for testing this assumption and quantifying the related uncertainties in this system so that further research may derive conclusions about the results presented here. A framework based on Bayesian Inference is implemented to quantify these uncertainties.

## 2. Quantifying Uncertainty

### 2.1 Proposed Methodology

The following methodology for solving the problem of quantifying the uncertainties that appear in a cable's self-damping behavior is proposed:

1. Gather experimental data for the phenomenon under study via an agreed-upon experimental method.
2. Put those measurements in the context of a model, be it analytical or computational, that approximates the studied phenomenon.
3. Use Bayesian methods to calibrate the model's parameters.
4. Obtain a description of the parameters and phenomenon. This then allows a classification and quantification of the two types of uncertainty.

This methodology is on par with most literature on Bayesian model calibration [15], and it does not propose anything new. However, this kind of analysis has seldom been applied to cable mechanics. It is then interesting to apply this methodology to this field to test long-held assumptions about the cable self-damping that appear in literature and most practical applications.

### 2.2 Self-Damping Measurements

The cable tested is an OPGW type, composed of two layers of aluminum wrapping steel and aluminum alloy wire and a core where an aluminum casing surrounds several layers of polymeric materials and optical fiber wires. Configuration details are shown in Fig. 2 and Table 1.

In the test span, according to Fig. 3, the effect of the wind on the cable is replicated, generating vibrations on it. This vibration energy is counter-balanced with the self-damping of the cable, as no additional dampers are present. When moderate wind speed conditions occur (lower than 7 m/s), Von Karman vortex shedding will induce vibration at frequencies depending on the Strouhal relationship. This nondimensional number is approximately 0.185 for all typical power lines cables [16]. The shaker is manually controlled through a variable-frequency drive (VFD). By adjusting the drive frequency of the cable, its resonant frequencies can be tuned. The excitation force is measured with a load cell.

Since the system is sensitive to the variability of the tension load, a closed-loop control system keeps the tension within a specific range. With the measurement provided from the tension cell, the system constantly applies adjustments with a linear electric actuator to the lever arm. The methodology specified in the standards [17] to characterize the power dissipation capacity of overhead conductors and cables are the Inverse Standing Wave Method (ISWR) and the Power Method (PT). The Power Method was used for the OPGW cable studied in this work. In this method, the cable is mounted in the test workbench and forced to vibrate in one of its natural frequencies at the prescribed vibration amplitude.

Since the cable's response is non-linear, it may not always be possible to produce pure sinusoidal signals at resonance. Therefore, a Fourier Transform was applied to the signal to obtain the amplitude and phase of the principal vibration component.

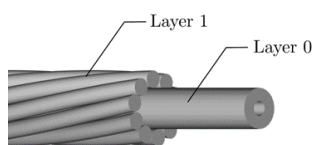


Fig. 2. OPGW Cable.

Table 1. Geometric Configuration of OPGW Cable

Layer No.	Wire Nos.	Wire dia. [mm]	Material
0	1	8.30	Aluminum Alloy
1	10	3.55	Aluminum wrapping steel



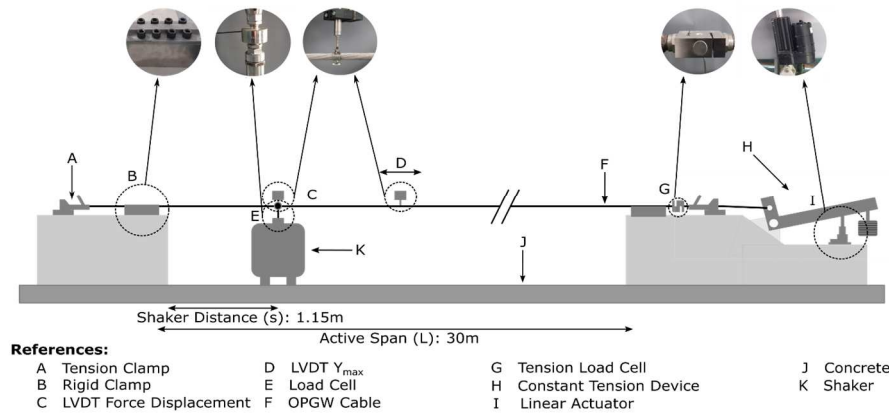


Fig. 3. Experimental Setup.

When a stationary condition is reached, the energy introduced by the shaker to the cable, over one cycle of vibration, is equal to that dissipated  $E_{diss}$  by the span. The energy introduced in the cable, and largely dissipated by its self-damping mechanism, is determined by measuring the force  $F$  acting between the cable and the shaker and the displacement of the driving point  $Y_f$ . For this purpose, a load cell and linear variable differential transformers (LVDT) sensor are installed at the driving point of the shaker, and the phase difference  $\theta_d$  between the signals is recorded. The following equation then gives the result:

$$E_{diss} = \pi \cdot F \cdot Y_f \cdot \sin \theta_d \quad (1)$$

The test procedure requires the location of middle-span antinodes and the following adjustment of antinodal amplitude to reach the prescribed level  $Y$  for every tunable resonance frequency  $f$ . Finally, the power dissipated by the cable  $P_{diss}$  is calculated by the following equation:

$$P_{diss} = f \cdot E_{diss} \quad (2)$$

During the experimental test, all variables (excitation force, tension load and displacements) are recorded with a QuantumX data acquisition system [18], and post-processed with signal processing software developed ad hoc.

### 2.3 Analytical Model

Modeling the self-damping of a cable has been a subject of debate for the last 30 years. Many mechanical models have been developed to address this based on distinct mechanisms. Noiseux [19] adopted a tensioned-beam continuous model with a complex bending stiffness to describe the hysteretic bending behavior of stranded conductors. Within this context, the cross-sectional energy dissipation is controlled by a hysteretic loss factor, a function of the vibration amplitude. Expressions for the dissipated power are derived from the model, and by using the ISWR method, the dependency of the hysteric loss factor and frequency can be established. Foti and Martinelli [20] developed a unified approach to cable-self damping based on the flexural rigidity of a conductor and the changes that it experiences during bending due to the hysteresis cycle of the cable. However, there is no agreed-upon model for self-damping, and it is necessary to rely on international standards like. The recommended model is the empirical Power Law Eq. (3). The parameters for this equation are usually obtained via regression techniques. This model shows the antinode displacement to cable diameter ratio  $Y = y/D$ ,  $f$  is the vibration frequency  $f$ , and  $T$  is the tension the cable was subject to:

$$\frac{P_{diss}}{L} = k \frac{Y^l f^m}{T^n} \quad (3)$$

Empirical models have no basis in physical law other than observations and intuitions from the modelers. It is then difficult to disregard their predictions since the parameter space has more freedom to adjust itself to observations. Analytical models do not pose this difficulty since the disagreement between model and observations often implies that the underlying reasoning for posing the model was incorrect. Empirical models should then be tested based on their quantified uncertainties about observations.

### 2.4 Probabilistic Model

This paper's main calculation's objective is to quantify the uncertainties related to every parameter in the Power-law model. Bayesian statistics have a long story with model calibration and uncertainty quantification. Recent developments in open-source libraries for probabilistic programming have made these techniques more readily available to the scientific public. The proposed framework relies on the Python library PyMC3 [21], used for probabilistic programming and Bayesian inference. The methodology is as follows:

1. Propose prior probability distributions for each parameter of interest in the model.
2. Propose a Likelihood probability distribution.
3. Use the Power-Law model as a mean for the Likelihood distribution and incorporate the observed data.
4. Apply a sampling algorithm to sample the posterior distribution of the desired parameters obtained by applying Bayes' theorem.
5. Post-process the results.

To state it more rigorously: Given a set of observations of the desired quantity and the independent variable associated with it: and a model  $\mathcal{M} = \mathcal{M}(\mathbf{x}, \theta_{\mathcal{M}})$  that depends on some parameters and some variables, the likelihood function for the observations given the parameters can be established as:  $\mathcal{L}(\mathcal{D} | \mathcal{M}(\mathbf{x}, \theta_{\mathcal{M}}), \theta_{\mathcal{L}})$  for some distribution. It is then possible to apply Bayes' Theorem using this likelihood function and data to obtain the posterior distribution for the parameters of the model and likelihood:



**Table 2.** Algorithm 1: Iterative Approximation of Posterior Distribution

1	<b>procedure: Model Initialization:</b>	
2	$\theta_M \sim \Pi_1(\theta)$	Model Parameters
3	$\theta_L \sim \Pi_2(\theta)$	Likelihood Parameters
4	$\Pi(\theta_L, \theta_M   \mathbf{x}, \mathcal{D}) _{i=0} \leftarrow$ Bayes Theorem	
5	<b>procedure: Progressive Approximation</b>	
6	<b>for</b> $i = 1 \dots \text{Max}_{\text{iter}}$ <b>do:</b>	
7	$\theta_L, \theta_M \sim \text{Interpol}(\Pi(\theta   \mathbf{x}, \mathcal{D}) _{i-1})$	
8	$\Pi(\theta_L, \theta_M   \mathbf{x}, \mathcal{D}) _i \leftarrow$ Bayes Theorem	
9	Calculate Performance Metrics	

$$\Pi(\theta_L, \theta_M | \mathbf{x}, \mathcal{D}) = \frac{\mathcal{L}(\mathcal{D} | \mathcal{M}(\mathbf{x}, \theta_M), \theta_L) \Pi(\theta_L, \theta_M)}{\Pi(\mathcal{D})} \tag{4}$$

This result is intractable by any analytical means, so it requires the aid of sampling algorithms to get the shape of the said posterior distribution. It is possible to relate aleatory uncertainties to the Likelihood’s standard deviation and degrees of freedom and epistemic uncertainties as originating from the probability distributions from the Model’s parameters calculated via the Bayes Theorem.

The numerical requirements for these calculations made it necessary to propose an iterative procedure to get the final posterior distributions for the parameters. In this way, the sampling process was applied to an initial model, and the results transformed into an interpolated distribution for the following steps. Thus, convergence can be evaluated.

### 2.5 Implementation

For this paper, the model  $\mathcal{M}$  is the empiric Power Law model of Eq. (3). The independent variables in this model are  $\mathbf{x} = (y, f, T)^i$ . The observed quantity  $y$  is the power dissipated per unit length. The model parameters  $\theta_M$  upon which inference is performed are the exponents:  $l, m, n$  and the proportionality constant  $k$ . The Likelihood function was chosen as a Student’s T distribution with parameters  $\theta_L = (\mu, \nu, \sigma)^i$  as mean, degrees of freedom, and standard deviation, respectively. The mean  $\mu$  is defined by Eq. (3). This approach is standard in Bayesian linear regression, where the regression line is supposed to be the mean for the observed data. The approach here is similar to the relationship under study, the Power Law, which is proposed to be the mean for the observed data. The most widely used sampling algorithms have shown difficulties in navigating the distribution given the non-linear mean that the Power Law model defines. For this reason, the Sequential Monte-Carlo (SMC) [22] sampling algorithm was used. The SMC sampler is included in the class of Approximate Bayesian Computation methods (also called likelihood-free inference methods), a group of techniques developed for inferring posterior distributions in cases where the likelihood function is intractable or costly to evaluate. SMC combines several statistical ideas, including importance sampling, tempering and an MCMC kernel. Tempering is a process where an auxiliary temperature parameter is used to control the sampling process. This is possible to see if the posterior is expressed as:

$$p(\theta | y)_\beta \propto p(y | \theta)^\beta p(\theta) \tag{5}$$

When  $\beta = 0$  then  $p(\theta | y)_{\beta=0}$  is the prior distribution and when  $\beta = 1$  the true posterior is recovered. This can be useful as in general sampling from the prior is easier than sampling from the posterior distribution. Thus,  $\beta$  can be used to control the transition from an easy to sample distribution to a harder one.

### 2.6 Convergence and Performance Criteria

Markov Chain Monte Carlo (MCMC) methods are based on sampling from distribution until the sampled population accurately represents the target distribution. This kind of iterative behavior often warrants the question of when to stop the simulation, i.e., what convergence criteria should be applied to the problem of sampling the target distribution. There are two main methods used to assess convergence: The Gelman-Rubin statistic and the Markov Chain Standard Error.

The Gelman-Rubin Statistic was first described in [23] and corrected in [24]. It describes the potential reduction scale for the variance of the target distribution that further drawing samples would produce. Procedure to calculate it is as follows:

1. Simulate  $m \geq 2$  sequences of length  $n$ .
2. For each scalar parameter of interest, compute:  $B/n$  as the variance between the  $m$  sequence means and  $W$ , the average of the variances based on  $n - 1$  degrees of freedom.
3. Estimate the target mean  $\hat{\mu}$  by the sample mean of the  $mn$  simulated parameters.
4. Estimate the target variance by a weighted average of  $W$  and  $B$ :  $\hat{\sigma}^2 = (n - 1)W / n + B / n$
5. Estimate what is known about the studied parameters by approximating the knowledge about the parameters (recall that probability in the Bayesian sense implies knowledge about something) in the form of a Student’s T distribution with center  $\hat{\mu}$ , scale, and degrees of freedom.

Finally, the Gelman-Rubin statistic,  $\hat{R}$ , can be calculated as the ratio of the variance estimate and the within sequence variance  $W$  plus an additional term that includes more variance from the usage of a Student’s T distribution. This is:

$$\hat{R} = \frac{d + 3 \hat{V}}{d + 1 W} \tag{6}$$

The value of  $\hat{R}$  tends to one as  $n \rightarrow \infty$ , a high value of  $\hat{R}$  implies that the simulation should be run further. Once  $\hat{R}$  reaches 1 then the sampled distribution correctly represents the target.



The other method, Markov Chain Standard Error (MCSE), was developed to assess the convergence of MCMC computations. The objective of MCMC computation is to produce an estimator  $g_n := (\sum_{i=1}^n g(X_i))/n$  of the quantity  $E_{\pi}g = \int_{\mathcal{X}} g(x)\Pi(dx)$  for some function  $g$  and some distribution  $\Pi$ . The MCSE is then computed as which a priori cannot be calculated since  $E_{\pi}g$  is unknown. It turns out that by some regularity conditions, the MCSE admits a central limit theorem, and the following expression arises [25]:

$$\sqrt{n}(g_n - E_{\pi}g) \rightarrow N(0, \sigma_g^2) \tag{7}$$

Thus, by estimating the variance  $\sigma_g^2$  its possible to estimate the MCSE. The calculation for  $\hat{R}$ , mean and standard deviation for the MCSE for this paper was done by the Python package ArViz [26].

### 3. Results and Discussion

#### 3.1 Description

Results will consist of four parts. First, the prior distributions are presented. Following are the results from the final iteration and convergence process. Afterwards, the performance metrics' plots for both chosen metrics are presented alongside tables summarizing the first and final iteration. A comparison between the obtained experimental data and model predictions is then addressed. Finally, an analysis of the uncertainty regions of the model is presented.

As for the algorithm implementation details, the SMC sampler was run for 5500 draws and four chains per iteration. There was a total of 4 iterations for a total of 120000 draws. At the end of each iteration, performance metrics were recorded to monitor convergence, and the algorithm stopped once the metrics reached the desired threshold.

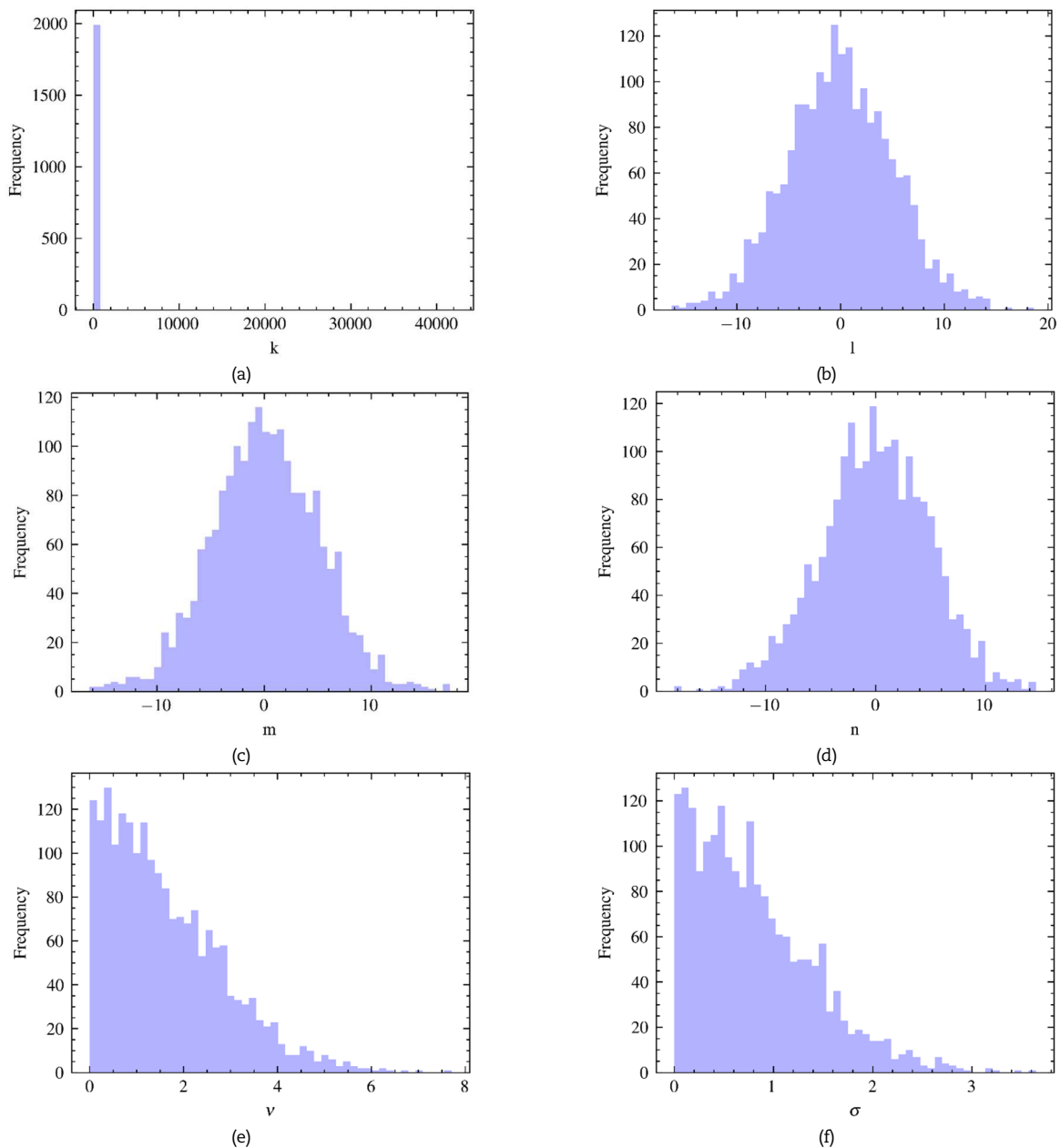


Fig. 4. Prior Distribution for relevant parameters.



**Table 3.** Summary of the results after the first Iteration

	Mean	Standard Deviation	3% Percentile	97% Percentile	MCSE Mean	MCSE SD	$\hat{R}$
$k$	4.138	6.228	0.028	11.917	0.193	0.138	1.11
$l$	3.065	0.323	2.465	3.711	0.004	0.003	1.01
$n$	2.389	0.415	1.606	3.167	0.002	0.002	1.01
$m$	5.074	0.552	4.066	6.126	0.003	0.002	1.0
$v$	2.424	0.958	0.912	4.217	0.193	0.138	1.11
$\sigma$	0.094	0.02	0.047	0.12	0.006	0.005	1.0

**3.2 Prior Distributions for the parameters**

The first step in any Bayesian analysis is to quantify what preexistent knowledge is held about the model in probability distributions about the parameters. There are two main things to worry about when stating these distributions; firstly, it is essential to be vague enough about the value of the parameters. Because a real danger in this kind of analysis is confirmation bias, i.e., constraining the prior to a preferred zone and then getting results in that zone may underestimate the underlying uncertainties. Secondly, constraints should be placed to a sensible interval for the priors. One reason for this is that the algorithms often employed for inverse problems like the one in this paper suffer greatly from non-convergence due to the probability space not being sufficiently specified. Another issue is that these are expensive and time-consuming calculations, so effort should be put into optimizing the use of resources in a meaningful space. It is then necessary to resort to a mixture of expertise and intuition about how to state these prior to accommodate the two stated criteria. Here is where the probabilistic-programming framework of PyMC3 shines the most, allowing one to freely state the prior distributions in a straightforward and easy-to-implement manner.

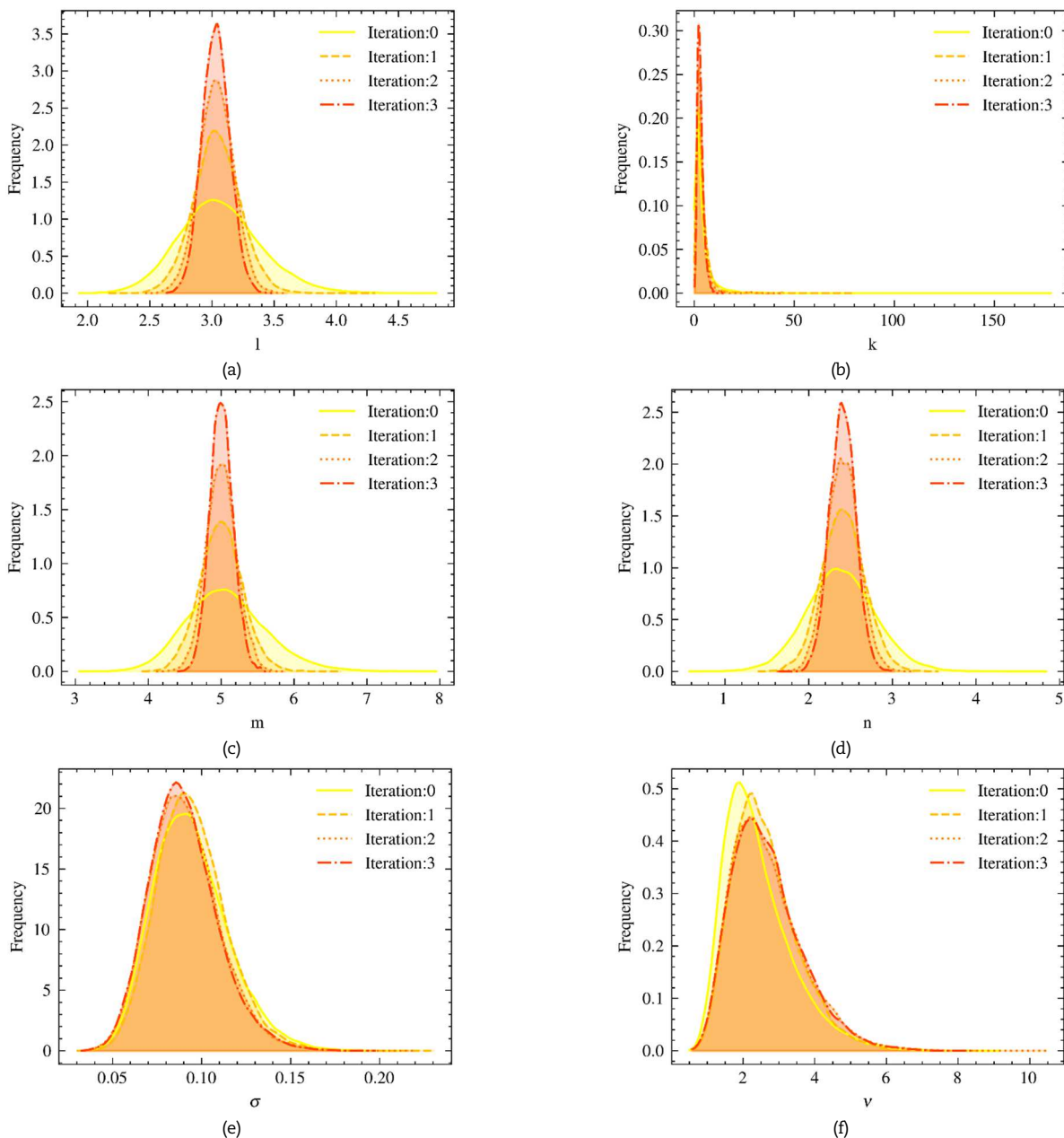


**Fig. 5.** Convergence Process.



Table 4. Summary of the results after 4 iterations

	Mean	Standard Deviation	3% Percentile	97% Percentile	MCSE Mean	MCSE SD	$\hat{R}$
$k$	3.155	1.629	0.733	6.285	0.01	0.007	1.0
$l$	3.03	0.11	2.825	3.239	0.001	0.0	1.0
$n$	2.405	0.154	2.118	2.698	0.001	0.0	1.0
$m$	5.005	0.159	4.709	5.309	0.001	0.001	1.0
$\nu$	2.675	0.981	1.037	4.5	0.006	0.004	1.0
$\sigma$	0.09	0.019	0.055	0.126	0.0	0.0	1.0

The initial prior distributions for the model initialization procedure were chosen to be Normal for the exponents, a positive-bounded Cauchy distribution for the proportionality constant and a positively bounded Normal distribution for the likelihood parameters:

$$k \sim \text{HalfCauchy}(\beta = 5) \tag{8}$$

$$n, l, m \sim \mathcal{N}(\mu = 0, \sigma = 5) \tag{9}$$

$$\nu, \sigma \sim \text{Half}\mathcal{N}(\sigma = 2) \tag{10}$$

In this way, an equilibrium between the non-specificity of the prior (as not to influence the posterior) and giving the sampling algorithm a relevant probability space to sample is structured. Figure 4 shows these distributions.

### 3.3 Simulation process

Studying the convergence process in this kind of algorithm is interesting because it provides a clear view of how the initial model performed as a starting point for the calculation. Figure 5 omits the prior distributions and presents the results after the end of the first iteration. In this way, the uncertainty for the parameters is indeed quantified because possible to visualize how adding more samples contributes less and less to reduce the confidence intervals for the distributions. Tables 3 and 4 summarize the results of the first and last iterations. The values presented there comprise confidence intervals, mean, standard deviation, and the required performance metrics.

### 3.4 Performance Metrics

The study of convergence is crucial here; of note is the relation between both contemplated metrics and the overall convergence of the distributions. As seen in Figs. (6) and (8), the complete inference process converges once all variables reach an acceptable threshold. There is evidence that the parameters under study are not multimodal since the value would not tend to one since the sampler would get stuck in the different regions defined by the modes.

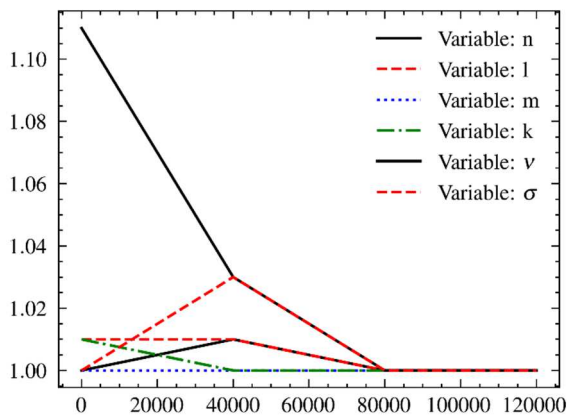


Fig. 6. Gelman Rubin Statistic vs. Number of Draws.

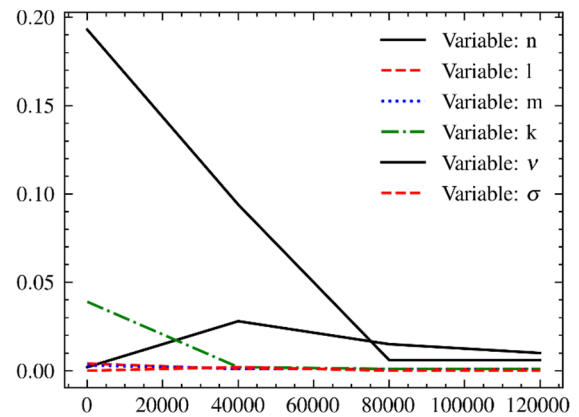


Fig. 7. Markov Chain Standard Error Mean vs. Number of Draws.

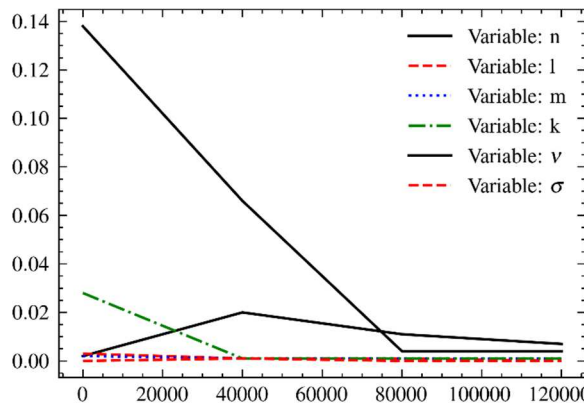


Fig. 8. Markov Chain Standard Error Standard Deviation vs. Number of Draws.



### 3.5 Posterior Distributions

Further insight into the model can be found by analyzing the joint probability distributions of the distinct parameters; this serves to study which combinations of parameters are more likely and if there is any correlation between parameters. Figure 9 shows that every distribution except for parameter  $k$  is symmetrical and unimodal around a mean value. This is an important feature because it speaks about convergence of the result to a particular value and the width of the distribution represents the epistemological uncertainty about the value. Distribution for  $k$  presents the most interesting results. As pointed out before, this parameter is usually lacking from the reports of experimental data, this is mainly because its value is a difficult thing to estimate since it not only depends on the measurement system but the fact that it is even a constant is disputed in other literature [27]. From the point of view of the analysis presented here, unexplained variations in  $k$  could be assigned to its epistemic uncertainty and further functional dependence on other variables can also be assigned to other variables' exponents uncertainty. In this sense then it is no longer necessary to pose contrived empirical models when it is possible to evaluate the epistemic uncertainty of the model and judge its results based on it.

Other minor comments include the fact that there exists slight correlation between the  $l$  and  $m$  exponents. This may be a consequence of the coupling that exists between resonant frequency and antinode amplitude since loop length decreases with higher frequency and antinode amplitude is bounded by loop length.

### 3.6 Comparison with Experimental Data

Since every variable in the proposed model is random, the predicted dissipated energy is then a deterministic random variable. To present this, Fig. 10 shows dissipated power versus the amplitude to diameter ratio for the complete frequency spectrum under study. The model lines represent the value of the Power Law evaluated at the predicted mean for every parameter.

### 3.7 Uncertainty Regions

Another way to evaluate this model is via analyzing how its error bars change with frequency, amplitude, and iteration of the model. Error bars are used as another way to evaluate convergence and to identify regions where the model struggles to get accurate results. The easiest way to do this is to evaluate the models at the percentiles of choice for the random variables representing the model's parameters; thus, a confidence interval of sorts is established, and the different regions are identified. This analysis is presented in Fig. 11 for the first and last iterations. The confidence interval was obtained by adding and subtracting one standard deviation for the mean of each parameter and evaluating the model in the same way as in section 3.6.

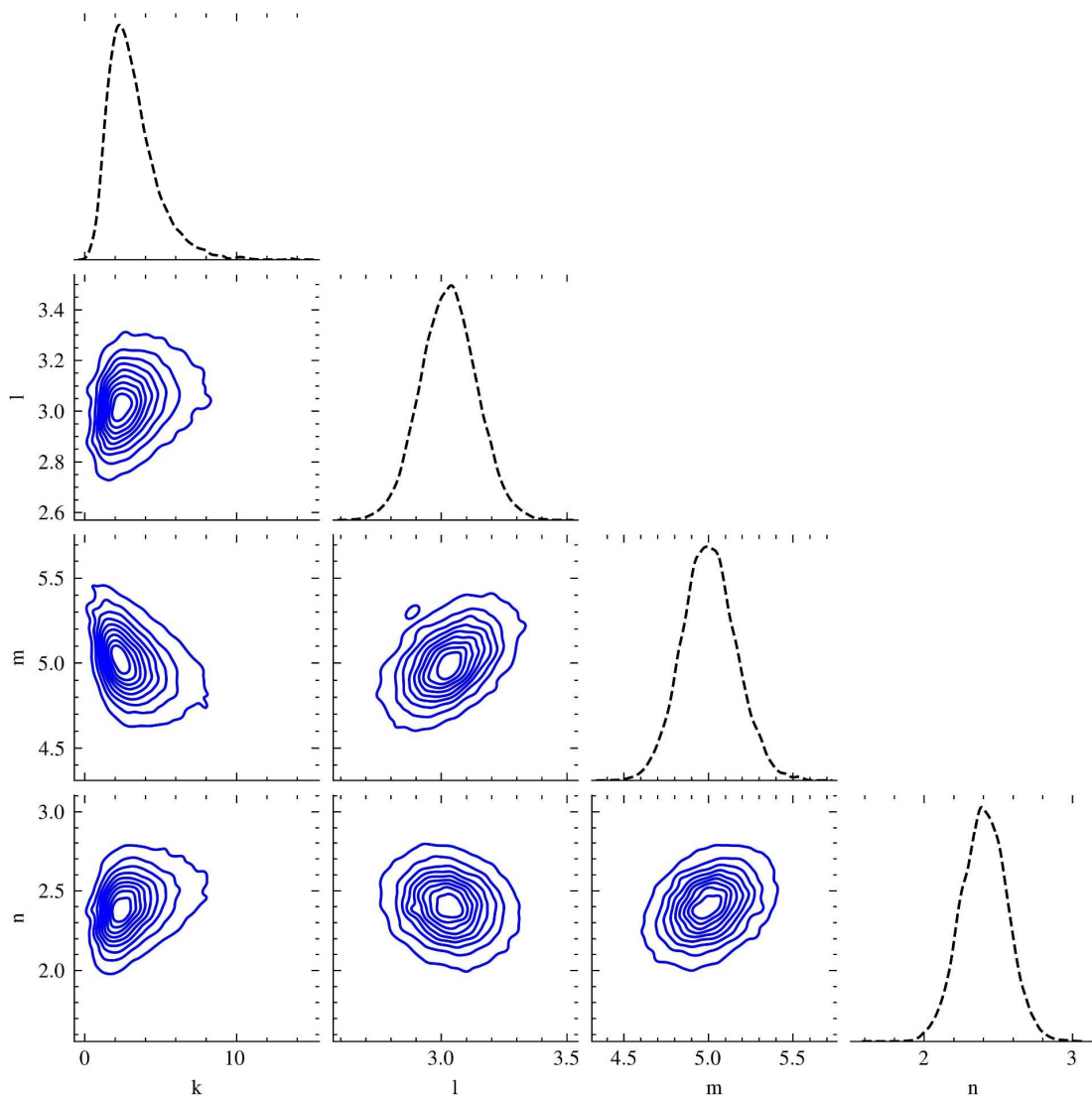


Fig. 9. Posterior Distribution for relevant parameters after 4 Iterations of the Algorithm and kernel density estimation for the joint probability distributions for each pair of parameters.





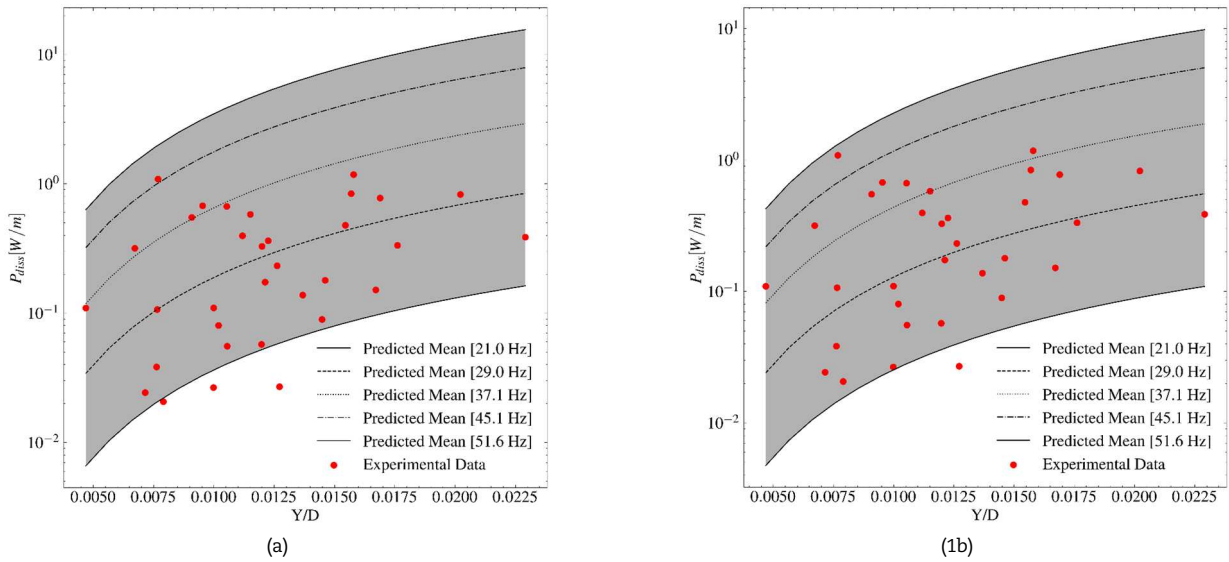


Fig. 10. Comparison between Experimental data and the model at the first iteration (a) and the final iteration (b). The grey region in both figures represents the whole frequency spectrum contemplated in this analysis.

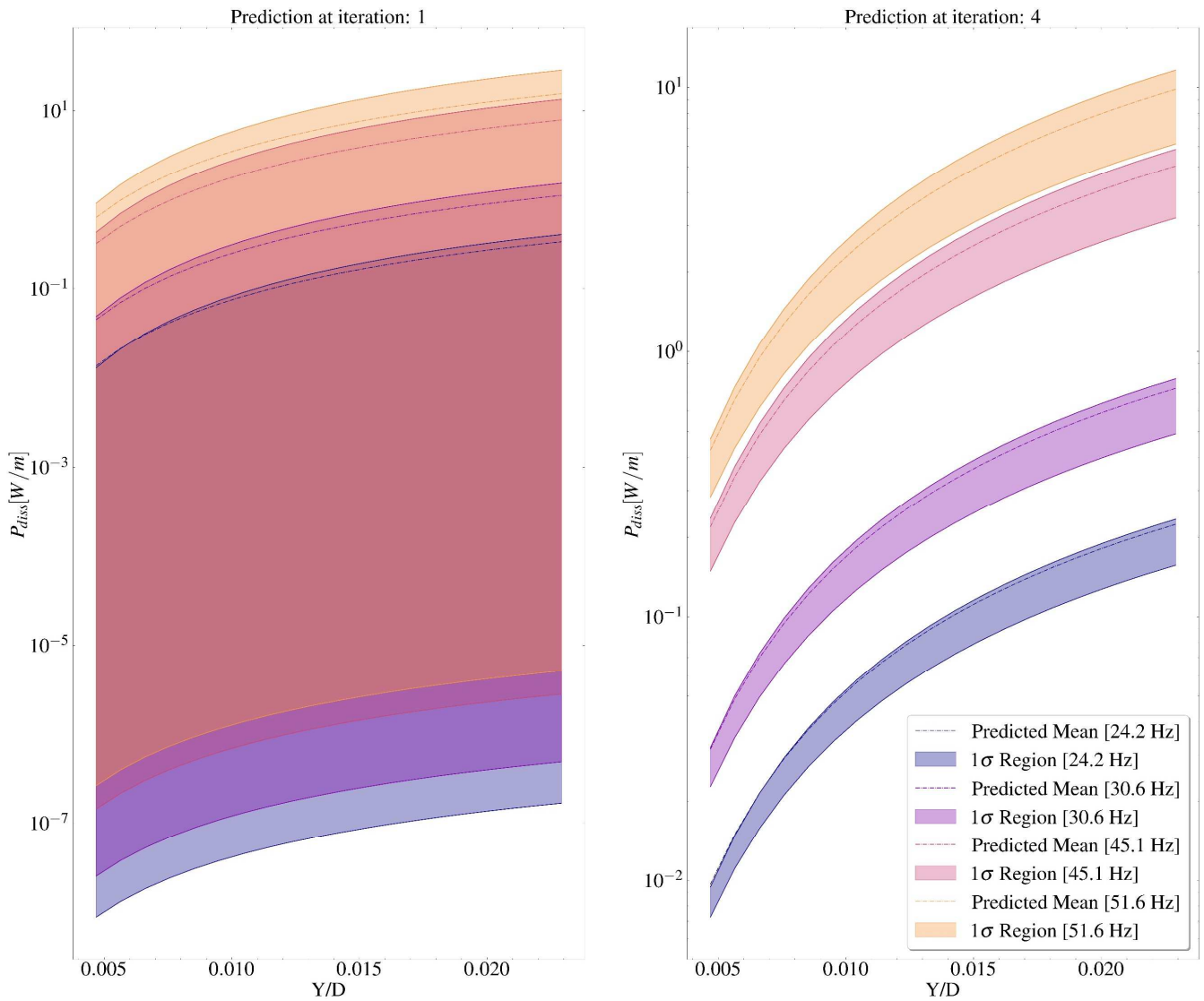


Fig. 11. Comparison of error bars at different frequencies for the whole amplitude spectrum at the first iteration (left) and the final iteration (right). The different colored regions represent the 1 region of uncertainty in prediction for each plotted frequency as a function of the parameter Y.



### 3.8 Discussion

State of the art regarding cable self-damping was one of the main reasons for the experimental section of this work. Experimental results available in the literature for cable self-damping are quite restrictive in scope and mostly are available Aluminum Conductor Steel Reinforced (ACSR) conductors. The only experimental work available for OPGW cables is published by Tavanno [28]. The main problem with these results is the lack of different tensions used to calculate the cable's self-damping; this leads to the coefficient  $n$  not being assigned a value in the report. Other issues include the fact that the proportionality constant  $k$  is not included in the report, and neither are the measurement units used in the tests. This parameter lacking from experimental reports of cable self-damping is a common practice in this subject's literature.

Another aspect to be considered are the limitations of the power method used to obtain the experimental results, the applied variant of the method uses solid blocks as terminations. It is well known that cable loops near solid block terminations experience higher energy dissipations than their free vibrating counterparts. These extra energy dissipations affect the experiment's outcome and constitute part of the epistemic uncertainty of the model. This is because the Power Law model cannot account for these energy losses and the reported dissipated power should differ from the quantity experienced by an equivalent cable mounted in-service. Regardless of this limitation, the proposed methodology could quantify the uncertainties of the model. Further research should then focus on benchmarking the different proposed methodologies, e.g., Decay Method and ISWR, and rank them by their explanatory power using a Bayesian Model Comparison framework. This way, more definitive evidence about the different uncertainties of each experimental methodology could be obtained.

The cables also experience aerodynamic damping during their operation. To account for it during the study of cable vibration, it is a common practice to introduce a correction account for it in the energy balance method used to quantify the cable's vibrations. Even though aerodynamic damping should be accounted for as a sizeable source of energy dissipations, it was not the purpose of this work to study the whole phenomenon but instead to isolate the mechanical aspect of the process and quantify the uncertainties surrounding it [29].

The most agreed-upon practice in model calibration is to use prior distributions based on expert advice to gauge the region where the possible values of the studied parameters lie. Since an empirical model was being tested, it was the purpose of this work to use the most general priors possible to get the most unbiased results. This choice was quite successful since the analysis led to statistical evidence that the sign and approximate value of the model parameters agreed with the power Law model's initial formulation.

Good agreement between experimental data and the model was observed, and novel results were obtained regarding the confidence intervals of each parameter and how they influence the prediction of dissipated power. From there, it is possible to address the regions where the model exhibits different behavior. In the low amplitude and low-frequency zone, the model has few prediction problems, as shown by the amplitude of its error bar. In the medium frequency and medium amplitude zone, of significant interest for studying aeolian vibrations, the dispersion is small in proportion to the value of the predictions, so it is possible to rely on the model predictions here.

Finally, the large amplitude and high-frequency zones have the most considerable dispersion; this is likely because the amplitude depends on the loop length and the loop length decreases with frequency, making this zone quite difficult to sample experimentally.

## 4. Conclusion

The proposed approximation algorithm is helpful for sampling complex models since it provides a framework where the visualization of the results is readily available at each step. It allows for changing sampling parameters and even the sampling algorithm between iterations. Another critical aspect of the algorithm is that convergence metrics are evaluated at each step. These metrics are an essential part of evaluating the sampling process and the operating economics of the complex sampling algorithms involved. The overall evolution of the Gelman-Rubin statistic and the MCSE metrics were satisfactory, allowing for the early termination of the execution once the metrics reached a certain threshold. The proposed methodology successfully quantifies epistemic uncertainties in the form of parameter distribution and aleatory uncertainty in the form of likelihood distribution parameters.

### Author Contributions

D.F. Campos planned the scheme, initiated the project, suggested the experiments, and analyzed the empirical results; E.E. Löser developed the mathematical modeling and conducted the experiments; M.T. Pivon validated numerical results and provided the theoretical formulation. The manuscript was written through the contribution of all authors. All authors discussed the results, reviewed, and approved the final version of the manuscript.

### Acknowledgments

Not Applicable.

### Conflict of Interest

The authors declared no potential conflicts of interest concerning the research, authorship, and publication of this article.

### Funding

The authors received no financial support for the research, authorship, and publication of this article.

### Data Availability Statements

The datasets generated and/or analyzed during the current study are available from the corresponding author on reasonable request.



## Nomenclature


$B$	Variance between the $m$ sequence means	$\hat{V}$	Variance estimator for the Gelman-Rubin Student's T Dist
$D$	Set of tuples of observations and variables	$W$	Within Sequence Variance estimator
$d$	Degrees of Freedom for the Gelman Rubin Student's T	$Y$	Antinode amplitude to cable diameter ratio
$E_{diss}$	Dissipated Energy per vibration cycle by the span	$Y_f$	Driving point displacement
$E_{\pi g}$	Expected Value of operator $g$ under distribution $\pi$	$x$	Variables the model is conditioned upon
$F$	Applied force by the VFD	$\beta$	Tempering Parameter for the SMC
$f$	Cable Vibration frequency	$\theta$	Parameters for a PDF
$g_n$	Estimator for $E_{\pi g}$ at $n$ draws	$\theta_d$	Phase difference between $F$ and $Y_f$
$k$	Proportionality constant of the power law	$\theta_M$	Model Parameters
$\mathcal{L}$	Likelihood probability distribution	$\theta_L$	Likelihood Parameters
$l$	Antinode amplitude exponent	$\kappa$	Scale parameter for the Cauchy distribution
$\mathcal{M}$	Physical model under study	$\mu$	Mean for the Normal and Student's T Distribution
$m$	Vibration Frequency exponent	$\hat{\mu}$	Estimator for the sample's mean
$n$	Tension exponent	$\nu$	Degrees of freedom for the Student's T Distribution
$P_{diss}$	Power dissipated by the span	$\sigma$	Standard Deviation for the Normal and Student's T Dist
$p$	Probability density function	$\hat{\sigma}^2$	Estimator for a MCMC sequence's variance
$\hat{R}$	Gelman-Rubin Statistic		
$T$	Longitudinal tension the cable is subjected to		


## References

- [1] Günday, A., Karlik, S.E., Optical fiber distributed sensing of temperature, thermal strain and thermo-mechanical force formations on OPGW cables under wind effects, *8th International Conference on Electrical and Electronics Engineering (ELECO)*, 2013.
- [2] Kiessling, F., Nefzger, P., Nolasco, J.F., Kaintzyk, U., *Overhead Power Lines: Planning, Design and Construction*, Springer, Berlin Heidelberg, 2014.
- [3] Cosmai, U., Van Dyke, P., Mazzola, L., Lillien, J.L., *Conductors Motions in Overhead Lines*, Springer International Publishing, 2017.
- [4] Gasparetto, M., Falco, M., On vibrations induced in a cylinder in the wake of another due to vortex shedding, *Meccanica*, 9, 1974, 325-336.
- [5] Goldstein, S., *Modern Developments in Fluid Dynamics: An Account of Theory and Experiment Relating to Boundary Layers, Turbulent Motion and Wakes*, Clarendon Press, 1950.
- [6] Donohue Bishop, R.E., Hassan, A.Y., The lift and drag forces on a circular cylinder oscillating in a flowing fluid, *Proceedings of the Royal Society of London. Series A. Mathematical and Physical Sciences*, 277, 1964, 51-75.
- [7] Electrical Power Research, *Transmission Line Reference Book: Wind-Induced Conductor Motion*, 2006.
- [8] Campos, D.F., Ajras, A.E., Piovan, M.T., Bayesian model calibration for bending stiffness assessment in OPGW cables, *International Conference on Electrical, Computer and Energy Technologies (ICECET)*, 2021.
- [9] Hardy, C., Analysis of self-damping characteristics of stranded cables in transverse vibrations, *Proceedings of the CSME, CSME Mechanical Engineering Forum*, 1, 1990, 117-122.
- [10] Cardou, A., Jolicoeur, C., Mechanical Models of Helical Strands, *Applied Mechanics Reviews*, 50, 1997, 1-14.
- [11] Hardy, C., Leblond, A., On the Dynamic Flexural Rigidity of Taut Stranded Cables, *Fifth International Symposium on Cable Dynamics*, 2003.
- [12] Conseil International des Grands Réseaux Électriques (CIGRE), State of the art for testing self-damping characteristics of conductors for overhead lines, 2011.
- [13] International Electrotechnical Commission, IEC 62567-2013 - Methods for testing self-damping characteristics of conductors, 2013.
- [14] Oberkampf, W.L., Roy, C.J., *Verification and Validation in Scientific Computing*, Cambridge University Press, 2010.
- [15] Muehleisen, R.T., Bergerson, J., Bayesian Calibration - What, Why And How?, *International High Performance Buildings Conference*, 2016.
- [16] Diana, G., Falco, M., On the forces transmitted to a vibrating cylinder by a blowing fluid - Experimental study and analysis of the phenomenon, *Meccanica*, 6, 1971, 9-22.
- [17] Institute of Electrical and Electronics Engineers, IEEE Std 563: Guide on Conductor Self-Damping Measurements, 1978.
- [18] <https://www.hbm.com/es/>
- [19] Noiseux, D.U., Similarity laws of the internal damping of stranded cables in transverse vibrations, *IEEE Transactions on Power Delivery*, 7, 1992, 1574-1581.
- [20] Foti, F., Martinelli, L., A unified analytical model for the self-damping of stranded cables under aeolian vibrations, *Journal of Wind Engineering and Industrial Aerodynamics*, 176, 2018, 225-238.
- [21] Salvatier, J., Wiecki, T.V., Fonnesbeck, C., Probabilistic programming in Python using PyMC3, *PeerJ Computer Science*, 2(e55), 2016.
- [22] Lintusaari, J., Gutmann, M.U. Kaski, S., Corander, J., On the Identifiability of Transmission Dynamic Models for Infectious Diseases, *Genetics*, 202(3), 2016, 911-918.
- [23] Gelman, A., Rubin, D.B., Inference from Iterative Simulation Using Multiple Sequences, *Statistical Science*, 7(4), 1992, 457-472.
- [24] Brooks, S.P., Gelman, A., General Methods for Monitoring Convergence of Iterative Simulations, *Journal of Computational and Graphical Statistics*, 7(4), 1998, 434-455.
- [25] Flegal, J.M., *Monte Carlo Standard Errors for Markov Chain Monte Carlo*, University of Minnesota, 2008.
- [26] Kumar, R., Carroll, C., Hartikainen, A., Osvaldo, M., ArviZ a unified library for exploratory analysis of Bayesian Models in Python, *The Open Journal*, 4(33), 2019, 1143.
- [27] Wolf, H., Adum, B., Bozic, Z., The Impact of Empirical Rules for Aeolian Vibrations in Overhead Transmission Lines, *Transactions of FAMENA*, 34(2), 2010, 47-5.
- [28] Tavano, F., Collection of experimental data on aeolian vibration on single conductors, *CIGRE 22-91*, 1991.
- [29] Tavanno, F., Cloutier, L., Claren, R., Ervik, M., Hagerdorn, P., Hardy, C., Kern, G., Krispin, H.-J., Möcks, L., Rawlins, C.B., Dulhunty, P.W., Manenti, A., Tunstall, M., Asselin, J.M., Bückner, W., Havard, D.G., Hearnshaw, D., Diana, G., *Modelling of Aeolian Vibrations of Single Conductors*, Springer, 2018.

## ORCID iD

Damián Federico Campos  <https://orcid.org/0000-0002-4928-7941>

Enrique Eduardo Löser  <https://orcid.org/0000-0002-7117-1582>

Marcelo Tulio Piovan  <https://orcid.org/0000-0001-9464-1076>



© 2022 Shahid Chamran University of Ahvaz, Ahvaz, Iran. This article is an open access article distributed under the terms and conditions of the Creative Commons Attribution-NonCommercial 4.0 International (CC BY-NC 4.0) license (<http://creativecommons.org/licenses/by-nc/4.0/>).



**How to cite this article:** Campos D.F., Löser E.E., Piován M.T. Self-damping of Optical Ground Wire Cables: A Bayesian Approach, *J. Appl. Comput. Mech.*, 9(1), 2023, 205–216. <https://doi.org/10.22055/jacm.2022.40878.3666>

**Publisher's Note** Shahid Chamran University of Ahvaz remains neutral with regard to jurisdictional claims in published maps and institutional affiliations.

